

FREE UNIVERSITY OF BERLIN

Institute for Informatics



Bachelor thesis

study of Bioinformatics

**Model-based autosegmentation of brain
structures in the honeybee, *Apis mellifera***

Kerstin Neubert

August 21, 2007

Prof. Dr. Randolph Menzel^{1, 3}

Dr. Stefan Zachow^{2, 3}

Hans Lamecker²

Dr. Jürgen Rybak¹

¹Institute for Biology-Neurobiology, Free University Berlin

²Department of Visualization and Data Analysis of the Zuse Institute Berlin (ZIB)

³supervisors

Contents

- 1 Introduction** **1**
 - 1.1 Motivation 1
 - 1.2 Honeybee standard brain atlas 2
 - 1.3 Aim of this work 2

- 2 Foundations** **4**
 - 2.1 3D Reconstruction of Bee Brain Structures 4
 - 2.1.1 Confocal Imaging 4
 - 2.1.2 Aquisition of confocal Images 5
 - 2.1.3 Manuel segmentation of confocal images 5
 - 2.1.4 3D Reconstruction of individual Bee Brains 6
 - 2.1.5 Registration of Neurons into the Standard Brain 7
 - 2.2 Model-based segmentation 8
 - 2.2.1 Statistical 3D Shape Models 9
 - 2.2.2 Segmentation process 11

- 3 Automatic Segmentation of the calyx from confocal images** **12**
 - 3.1 Statistical 3D Shape Model of the calyx 13

3.2	Initialization by affine Registration	14
3.3	Grey value profile model	16
3.4	Displacement algorithm	17
4	Results	23
4.1	Evaluation	24
4.1.1	Symmetric surface distance	25
4.1.2	Volume overlap	25
4.2	Segmentation of training data	26
4.3	Extension of the calyx model	27
4.3.1	Compactness of the calyx model	27
4.3.2	Completeness of the calyx model	28
4.4	Segmentation of arbitrary test data	28
5	Discussion	36
6	Conclusions and Outlook	39
	Bibliography	41

List of Figures

2.1	Confocal image	5
2.2	Manual segmentation with the segmentation editor in Amira.	6
2.3	Honey bee Standard brain	7
2.4	Registered neurons into the honey bee standard brain.	8
3.1	Statistical shape model of the right median calyx	14
3.2	Variability of the statistical shape model.	15
3.3	Initialisation scheme for segmentation	15
3.4	Analysis of grey value profiles with Amiras ExamineProfileEditor	17
3.5	Grey value profiles and their derivatives.	18
3.6	Displacement of the calyx model in the image data	19
4.1	Segmentation process	31
4.2	Cumulative relative variance of the models containing 18 and 45 shapes	32
4.3	Leave-all-in segmentation and Leave-one-out segmentation with a model containing 45 training shapes	32
4.4	Manual and automatic segmentation of a confocal image	33
4.5	Manual and automatic segmentation of a confocal image 2	34

4.6 Leave-all-in segmentation and Leave-one-out segmentation with a
model containing 18 and 45 training shapes 35

List of Tables

4.1	Results of the Leave-all-in and Leave-one-out segmentations	27
-----	---	----

Acknowledgements

I would like to thank several people for their support during my thesis. Prof. Dr. Menzel for providing the lab space and him and Dr. Jürgen Rybak for the idea of the adaptation of the model-based segmentation method to insect brains. Hans Lamecker and Dr. Stefan Zachow for providing the methods and their continuous support. Heiko Seim and Dagmar Kainmüller for their help with the extension of the shape model and their support with Amira tools. Robert Brandt and Nicola Stollhof for the manual segmented honey bee brains.

Abstract

The honey bee standard brain (HBS) serves as a 3D platform for the visualization of neuronal morphologies of different brain preparations. The registration of single neurons into the HBS requires a time-consuming manual segmentation of neuropil boundaries in confocal image data. Therefore it would be desirable to automate the segmentation process. A model-based autosegmentation approach was successfully applied for medical data by Lamecker et. al [2]. This method uses a-priori information about the shape of the segmented structure and features of the image data during the segmentation process. In this work, I want to figure out, if this method can be adapted to confocal image data. Therefore I establish it for the segmentation of a single bee brain structure, the right median calyx. At first I was able to solve the problem of the initialization of the model-based segmentation by an affine registration of the individual confocal dataset to the standard grey value dataset. In order to enlarge the variability of an existing statistical shape model of the calyx consisting of 18 training shapes, I extended it by another 27 training shapes. For the adjustment of this model I analysed grey value profiles along surface normals of the training data. On the basis of a profile model I developed a displacement algorithm for the adjustment of the model to a confocal image dataset. Then I tested the automatic segmentation with the different sized shape models and the developed displacement algorithm for 45 confocal image datasets. In 80% of the segmentations, the result was good compared to the manual segmentations. In some cases the profile model failed. Furthermore there were sometimes large maximal distances between manual and automatic segmentation, because the profile model did not fit the particular profile. The segmentation result could be improved with the extended model.

Chapter 1

Introduction

1.1 Motivation

Because of its remarkable abilities in navigation, communication, visual and olfactory learning and memory processing, the honeybee, *Apis mellifera*, has become an interesting object for the research of the neuronal correlates of learning and behaviour. The workerbee's brain is smaller than $1mm^3$ and contains approximately 820000 neurons. It is used as a model for the study of elementary learning procedures at the level of single neurons and neural circuits. Due to the accumulated knowledge about its neuroanatomy the activity of single marked neurons can be analysed with electrophysiological recordings or optical imaging. Elementary neuronal processes are based on neuronal circuits consisting of many neurons. The synaptic conjunctions of the participating neurons have to be identified to model their interaction.

1.2 Honeybee standard brain atlas

In insects, neuroanatomical methods are used to interpret the results of intracellular staining of neurons which are part of the brain circuitry. But the study of parts of the neural network needs numerous preparations from different animals with different stained neurons. Due to the variable shape of the individual brains the relative spatial position of neurons stained in different preparations can not be easily determined. Therefore a 3D anatomical reference map is needed to integrate the whole data. This function is fulfilled by an average shape atlas of the honeybee brain, which consists of 22 segmented brain structures (neuropiles) computed from 20 beebrains, Brandt et. al 2005 [1]. The 3D honeybee brainatlas (HBS) helps to understand the 3D morphology, topographical relationships and putative connectivities of the neural network. The method of confocal microscopy was a prerequisite for the atlas generation, because it allows the recording of optical cross-section of whole brains without doing mechanical sections of the brain with light microscopy resolution. To integrate a stained neuron into the atlas, simultaneous staining of the neuron with a dye and immunostaining of its neuropil is done in the preparation. Then the neuropil outlines have to be manually segmented on every optical slice of the 3D data volume such that each voxel corresponds to a certain label for a neuropil. The resulting so called label fields are mapped to the corresponding standard brain labels by an affine and elastic registration. The computed affine transformation matrix and the deformation field are finally applied to the neuron to fit it into the atlas.

1.3 Aim of this work

Registration of single neurons in the honeybee brain atlas requires the time-consuming manual segmentation of neuropiles in confocal image data with the aid of visualization software Amira ¹. Statistical shape models are al-

¹Mercury Computer Systems, <http://www.amiravis.com/>

ready successfully used for the automatic segmentation of medical image data (CT) [2]. They model the variability of objects of a certain class by principle component analysis consisting of a small number of training shapes. In order to achieve a correct model of a biological structure one needs to find the anatomical corresponding points on all training shapes. In this work the model-based automatic segmentation strategy is applied to confocal image data. As a first approach the task of autosegmentation of neuropiles is focused to one brain structure, the calyx, which is a part of the mushroom body (see Fig.2.3). An already existing model of the calyx, which consists of 18 training shapes is extended by 27 shapes to improve its ability to adjust to shapes, that are not included in the model. For the adjustment of the model to the immuno-stained confocal data a displacement algorithm is established, which uses the features of the grey value profiles along the surface normals in each point for the suitable displacement. The method is tested for the automatic segmentation of immuno-stained confocal image data.

Chapter 2

Foundations

2.1 3D Reconstruction of Bee Brain Structures

2.1.1 Confocal Imaging

Confocal Laser Scanning Microscopy offers the acquisition of 3D image data of bee brains with high resolution providing an insight into the 3D morphology of neurons. A laser emits photons, which are focussed at a point in the object. The reflected fluorescence signal of the object is displayed through the lens at the pinhole and detected by a photomultiplier. The object is scanned in layers. Du to the focussing of the light structures beyond the focal plane are less illuminated and the fluorescent images are not focussed at the pinhole. Using a very good lens and a small pinhole single optical sections can be up to $1\ \mu m$ thick. After recording of the whole object, the 3D image stack is recomposed of all layers.

2.1.2 Aquisition of confocal Images

Dissected brains from adult, foragers honeybees were stained using a immunohistological protocol. They were treated with a primary antibody against synapse proteins (SYNORF1) and labeled with a fluorescent Cy3-conjugated secondary antibody. Whole mounts are imaged with a confocal laser scanning microscope. Fig. 2.1 shows sections of a confocal image stack of a synapsin stained bee brain. For more details see [1].

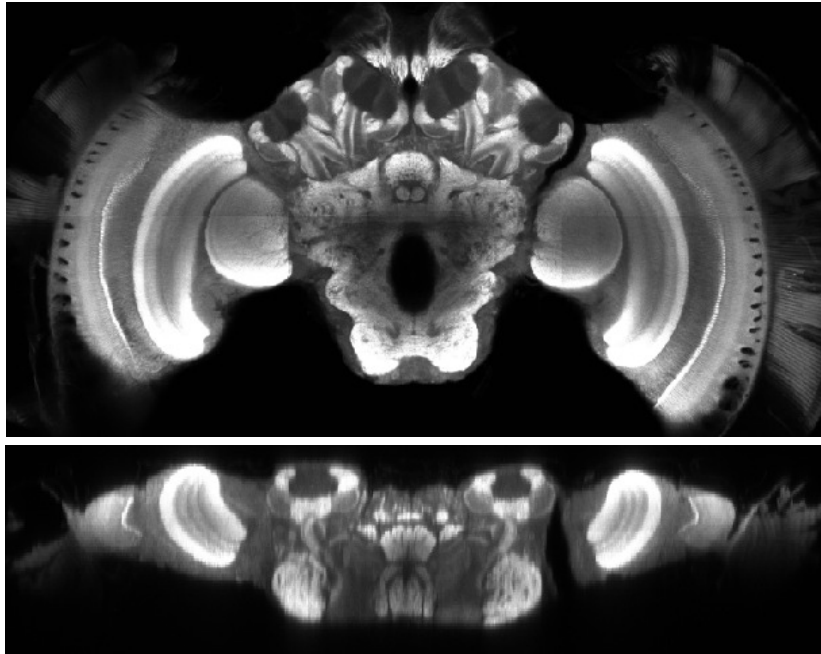


Figure 2.1: Frontal and horizontal grey value section from a confocal 3D image stack of synapsin stained bee brain

2.1.3 Manuel segmentation of confocal images

In immunostained confocal image stacks anatomically distinct regions of the bee brain were defined using the segmentation editor from Amira ¹. These so-called label fields are created by assigning voxels for each label, which

¹Mercury Computer Sysems, <http://www.amiravis.com/>

represent a coding for a particular brain structure (Fig.2.2). In the semi-automatic segmentation technique accurate free-hand manual segmentation are supported by tools provided by the Amira segmentation editor, such as edge-tracing and propagating contour, are used. For 3D segmentation interpolation between slices can be performed. These techniques have to be controlled carefully, because they tend to cut edges in the direction where the structure of interest is curved. For the neuropile analysed in this study (the calyces of the mushroom bodies (Fig.2.3) this is true at their distal ends. Amira allows the use of multiple label fields (22 materials in the HoneyBee Standard brain (HBS, Fig.2.3).

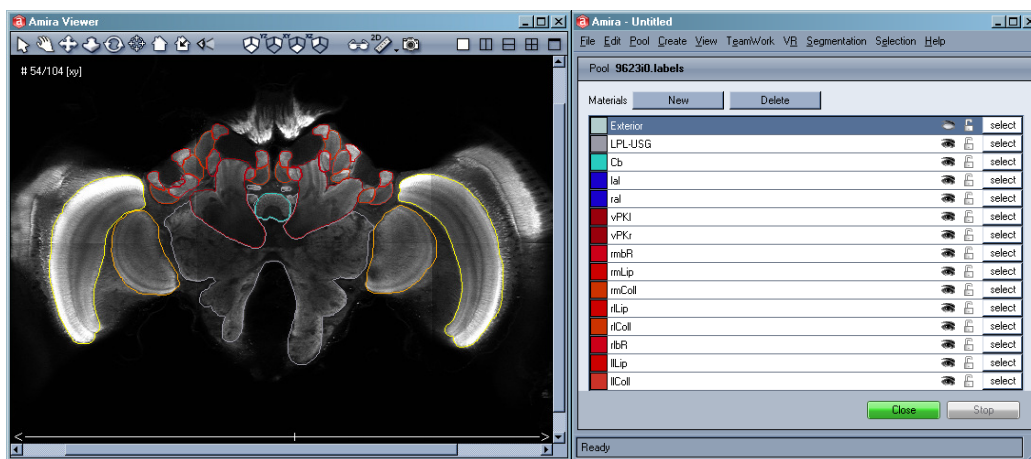


Figure 2.2: Manual segmentation with the segmentation editor in Amira.

2.1.4 3D Reconstruction of individual Bee Brains

On the basis of the 2D label fields the surfaces of 3D brain neuropiles are reconstructed. Triangular surface models, like the HBS, are representing the boundaries of the segmented structures. The boundaries are considered as interfaces between the different materials. In Amira a marching-cube algorithm is used, which extracts the boundary surfaces between the voxels belonging to different materials (labels). For a more detailed account on these issues see review by Maye et al. [4].

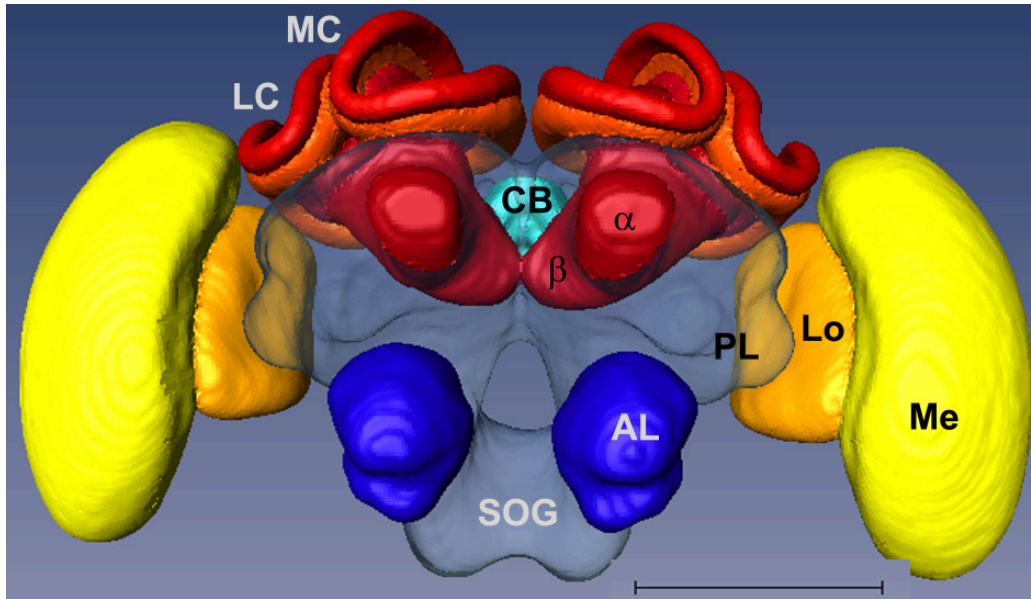


Figure 2.3: The Honey Bee Standard Brain (HBS). α : α lobe, β : β lobe, AL: antennal lobe, CB: central body, LC: lateral calyx, MC: median calyx, Lo: lobula, Me: medulla, PL: protocerebral lobe, SOG: suboesophageal ganglion, scale 500 μm

2.1.5 Registration of Neurons into the Standard Brain

A major use of the average shape-atlas of the honeybee is the fitting of individual neurons stained in different preparations into a common framework. That allows to perform a detailed comparative analysis of the topographical and fine structural details of neuron morphology (Fig. 2.4). Prerequisite for fitting neurons into the Standard Atlas is the accurate and reliable localization of region boundaries during the registration process (see chapter 1). This is true for manual (or semi-automatic) and fully automatic segmentation techniques, though the advantage of the latter is that interaction of human experts are reduced. Labeling performed by different segmenters often leads to variable results. Therefore it would be advantageous to use a-priori knowledge, as e.g. implemented in average shape models.

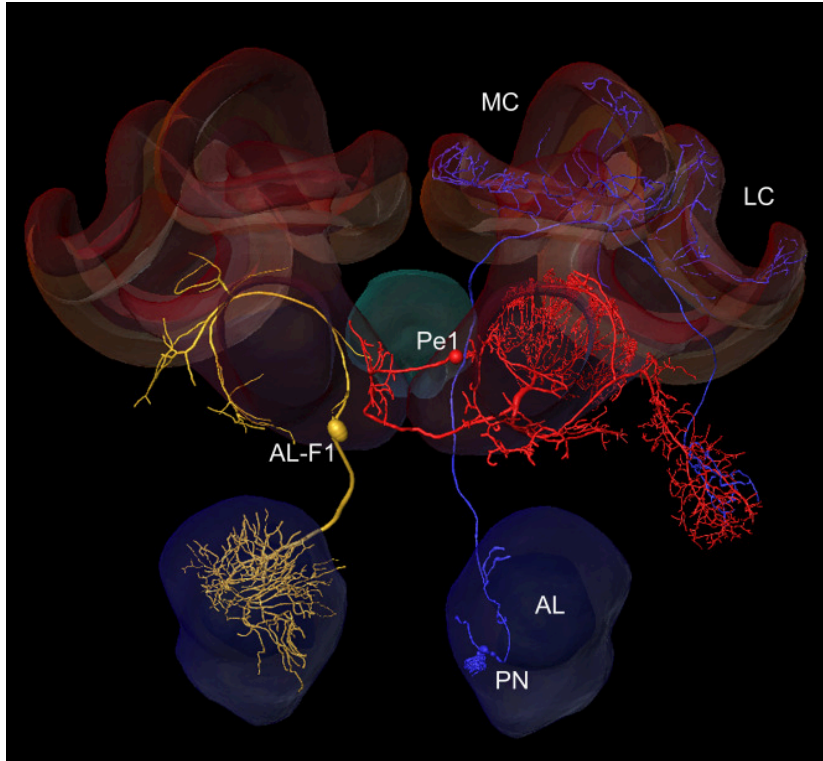


Figure 2.4: Identified neurons (AL-F1, Pe1, PN) registered into the honey bee standard brain. AL: antennal lobe, MC: median calyx, LC: lateral calyx. The optic lobes are omitted in this view. Figure provided by Neurobiology Lab Prof.Dr.Menzel

2.2 Model-based segmentation

Model-based segmentation combines apriori information about the 3D shape of already reconstructed surfaces with characteristic features of the image data. In this section the model-based segmentation method developed by Lamecker et al. is introduced ([2], [3]). In the first part the construction of 3D statistical shape models is described. The second part deals with the model-based segmentation process, which combines the 3D shape information of the generated statistical shape model with characteristic features of grey value profiles.

2.2.1 Statistical 3D Shape Models

Training Set

A 3D statistical shape model represents the mean shape and the shape variability of several individual surfaces from which it is made (training surfaces). The training shapes used for the modeling should be a good representation of the structure. They should not contain any artefacts, which could result in distortions in the statistic of the model. To obtain the training shapes, the image data is segmented and triangular surfaces are reconstructed from the labeled images. Then the surfaces are simplified, because the reconstructed surfaces contain mostly too much triangles, which contain no necessary information about the shape. In order to remove surface artefacts the training surfaces are smoothed.

Correspondence problem

For the construction of a statistical shape model from a set of training shapes the shape information of single surfaces has to be fused. The problem arises how shape information of the different surfaces should be combined to obtain a biological meaningful model. This results in the problem of finding anatomical meaningful correspondences between the training surfaces (correspondence problem). One solution is to divide all surfaces into the same characteristic regions homeomorph to a disc (named patches, see example in [fig.3.1](#) in chapter 3). One reconstructed model is selected as reference surface and remeshed to a homogeneous triangulation. Corresponding patches of the reference- and all training surfaces are matched to the unit disc (radius 1, centered in the origin). The reference patch serves as a common domain. Its triangulation is mapped to the geometry of all corresponding training patches. This results in equal number and arrangement but different locations of triangles in all surfaces i.e. each point of the reference surface has its definite counterpart in the remaining training surfaces.

Alignment

In the statistical analysis of the training shapes the spatial distances of a point in the training surface to its corresponding point in the reference surface is computed. Before this can be done, all surfaces must be located in the same coordinate system. For that purpose all training shapes are transferred to the coordinate system of the reference surface via a rigid transformation minimizing the distances between corresponding points.

Principle component analysis

Principle component analysis (PCA) is a method used to reduce the dimensionality of multidimensional data by preserving those features of the data, which show the greatest variance among the data. The mathematical definition of the PCA is a orthogonal linear transformation of the data to a new coordinate system in the way that the greatest variance of the data lies on the first coordinate (called the first principle component), the second greatest variance on the second coordinate, and so on.

Each triangular training shape S_i ($i = 1, \dots, N$) can be described via m discrete points on its surface resulting in a vector $v_i \in R^{3m}$. The corresponding points of the training shapes are modeled via principle component analysis (PCA). Each shape vector v_i sampled by m surface points $v_i \in R^{3m}$ can be expressed by the linear model:

$$v_i = \bar{v} + P b_i = \bar{v} + \sum_k p^k b_i^k \quad k = 1, \dots, m$$

whereas \bar{v} is the mean shape vector and $P = \{p^k\}$ the matrix of eigenvectors of the covariance matrix. The eigenvalues describe the variation in the direction of the associated eigenvectors. $b = \{b^k\}$ are the shape weights, which control the modes of variation. This results in a linear model of the shape variability of the training shape. It represents the mean shape \bar{v} of all surfaces from the training set with regard to a common triangulation

and the deviations from it contained in the shape modes \mathbf{b} of the variance P . The degrees of freedom of the model S are the shape parameters \mathbf{b} and the transformation \mathbf{T} :

$$S(\mathbf{b}, \mathbf{T}) = \mathbf{T}(\bar{v} + P\mathbf{b})$$

2.2.2 Segmentation process

At first the model must be roughly placed inside the segmented structure. Then the task is to find the form parameters \mathbf{b}^* and the transformation \mathbf{T}^* , which minimizes the distance of the model S to the autosegmented shape R :

$$(\mathbf{b}^*, \mathbf{T}^*) = \arg \min_{\mathbf{b}, \mathbf{T}} \|R - S(\mathbf{b}, \mathbf{T})\|^2 = \arg \min_{\mathbf{b}, \mathbf{T}} \|R - \mathbf{T}(v + P\mathbf{b})\|^2$$

The model adapts to the individual shape of the structure by an iterative adjustment of the position and the shape of the model with respect to the 3D image. In each iteration the one-dimensional gray value profiles along vertex normals for each vertex are computed. A displacement algorithm analyses these profiles and computes a suitable displacement vector for each vertex normal to the surface (Fig. 3.6). All displacement vectors form a vector field, which is applied to the vertices of the model. Based on the new shape the next iteration is computed. The shape of the model is limited by the variability of the training data, i.e. their shape parameters. In order to find a displacement algorithm, which uses information about the grey value profiles, the features of these profiles have to be modeled (profile model).

Chapter 3

Automatic Segmentation of the calyx from confocal images

The model-based automatic segmentation approach by Lamecker [2], which is explained in chapter 2 uses apriori knowledge about the shape of already reconstructed surfaces and features of the image data. This method is already in use for the segmentation of medical image data (CT, [2], [3]). The aim of this work is to adapt it for the segmentation of confocal images. I confine myself to the segmentation of one structure, the right median calyx, which is a part of the mushroom body of the bee brain. I extended an already existing 3D statistical shape model consisting of 18 training data by another 27 shapes and use it for the segmentation of calyces in confocal image data. The 3D model and the extension of its training set is described in section 1. Before the model-based segmentation process (chapter 2) can start the model has to be positioned within the segmented structure. The 3D image acquisition of medical data uses a reference coordinate system, which facilitate the initialization of the model in the data. Confocal imaging lacks such a reference system. The orientation of bee brains differs in confocal recordings. I found out, that an affine registration of the confocal image to a reference

image could compensate for this and initialize the model within the structure (section 2).

The shape model is adjusted to the individual grey value dataset via an analysis of grey value profiles along vertex normals for each vertex of the model surface. For each vertex of the model surface, a displacement algorithm computes the direction of a displacement vector normal to the surface using the current one dimensional gray value profile. The segmentation is an iterative process. In each iteration the shape parameters b and the transformation T of the model are modified with respect to the direction of the computed displacement vectors. For the segmentation of confocal images I analysed the grey value profiles in confocal images (section 3). On the basis of a profile model I developed a displacement algorithm (section 4).

3.1 Statistical 3D Shape Model of the calyx

For the extension of the calyx model I reconstructed the surfaces of manual segmented synapsin stained confocal images of forager bee brains. The confocal images and segmentations were provided by Robert Brandt and Nicola Stollhof. I simplified the generated triangular surfaces to 11000 triangles, because the original calyx model consists of about 10800 triangles. In order to find anatomical meaningful correspondences surfaces were divided manually into 6 regions (patches, Fig. 3.1) using the Surface Path Editor in Amira. The patch decomposition follows along recognizable shape features of the calyx surface. It was already defined in the original calyx model. The PCA analysis of the corresponding surface points was done from the 45 training shapes, resulting in a statistical shape model with 44 shape modes. The calyx model consists of the average shape and the principal variations of the training shapes contained in the eigenmodes. The degrees of freedom i.e. the shape parameters of the model are limited by the minimal and maximal shape parameters of the 45 training surfaces. The minimal and maximal variability of the three eigenmodes with the largest variance is shown in Fig 3.2.

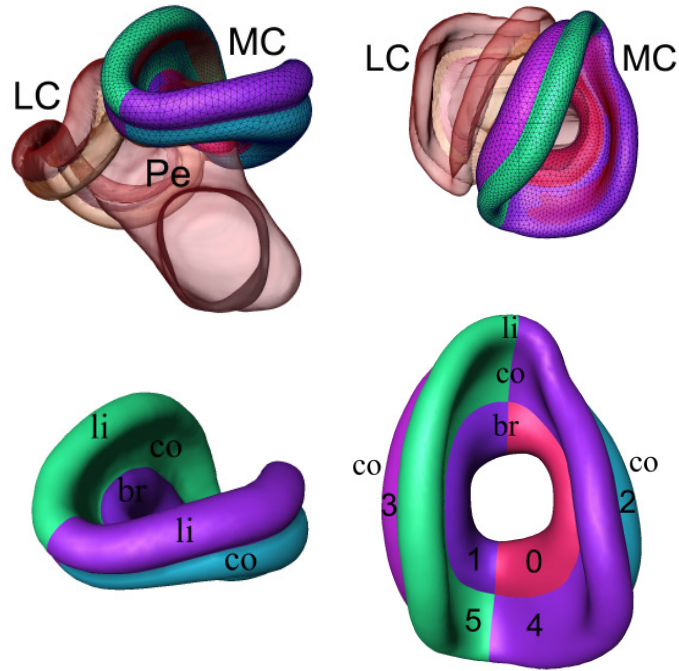


Figure 3.1: top: mushroom body with left and median calyx (LC, MC) and peduncle (Pe), lobes and calyx model; bottom: patch decomposition (0-5), lip (li), collar (co), basal ring (br)

The modeling process was done using the Amira visualization and modeling software.

3.2 Initialization by affine Registration

First of all the approximate localisation of the right median calyx in the 3D confocal image has to be found. This can be done by an interactive manual transformation of the mean calyx model in the 3D image. However, I use an affine registration of the 3D grey value image to the standard 3D grey value image. The parameters rotation, scaling and translation are optimized to maximize the correspondence between the grey value voxels of the two 3D data sets. In the parameter dialog of Amira's affine registration module I

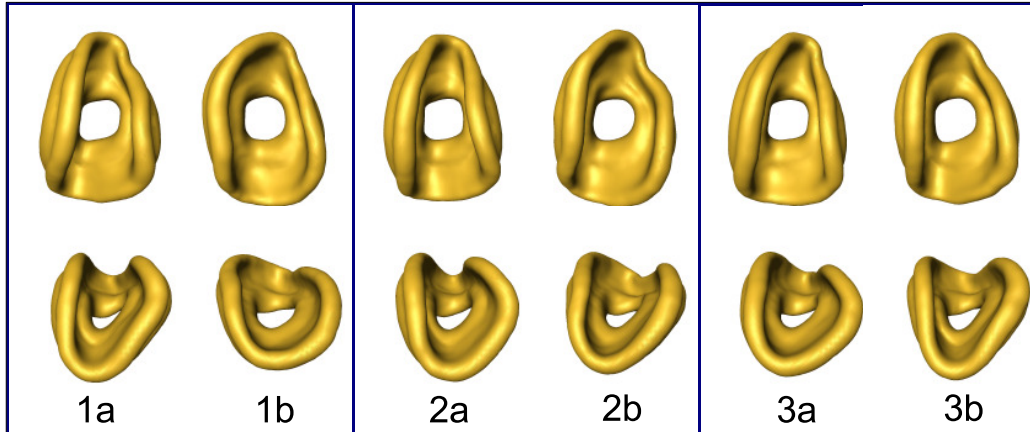


Figure 3.2: Variability of the statistical shape model of the calyx containing 45 training shapes: The minimal (a) and maximal (b) variability of the shape modes with the largest (1), second largest (2) and third largest(3) variance are shown in horizontal and frontal view

used the mutual information as a similarity measure. At first I transformed the calyx model in the Honey bee standard brain. Then the position of the calyx model in the 3D image is initialized by applying the inverse transformation matrix of the computed affine registration to the model (see Fig.3.3. Because individual bee brains differ in their anatomy, an affine registration is not sufficient for automatic segmentation. However, it suits well for the initialization of the automatic segmentation process.

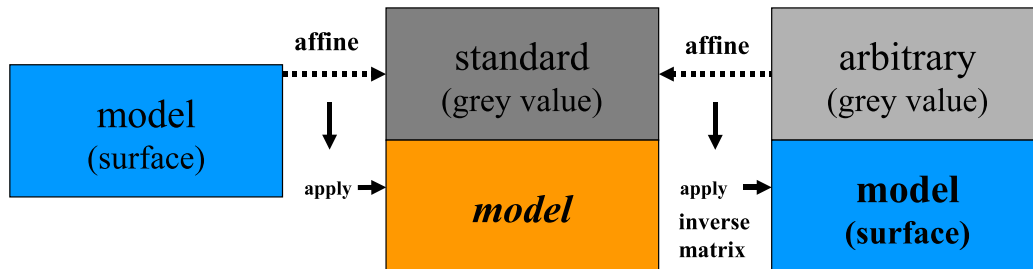


Figure 3.3: Procedure for the initialization of the calyx model in the arbitrary dataset: 1. affine transformation of the model to the honey bee Standard. 2. computation of the affine registration of the arbitrary dataset into the Standard grey value dataset, the inverse transformation of the affine registration is applied to the model.

3.3 Grey value profile model

The one-dimensional profiles along vertex normals of a training shape has characteristic recognizable features. The derivative of a grey value profile is the relationship between the height and the width of a peak in a grey value profile. Bright-dark transitions from inside to the outside of the calyx are visible as a maximum of the grey value profile inside the structure and a minimum outside. If the intensity of the grey values decreases, a minimum can be found in its derivative. If it increases, the derivative reaches a maximum. In Fig. 3.5 examples for grey value profiles and their derivatives in one confocal image dataset is shown. In order to develop a displacement algorithm for the adjustment of the calyx model to the grey value data, I analysed the grey value profiles and their derivatives along vertex normals of 10 already segmented confocal image datasets with Amira's ExamineProfile module (Fig. 3.4). The synapsin staining of the bee brains results in images with high contrast in the lip and basal ring subregions of the calyces (Fig. 2.1). Although a standardized protocol for the synapsin staining is used, the intensity of the grey values and the contrast varies between different preparation. Mostly the boundaries of the neuropiles are easily detectable by the synapsin staining, but the contrast varies significantly in depth because of an uneven penetration of the antibodies in the brain preparation. The grey value profiles are different in distinct regions of the calyx. For certain regions or patches I tried to classify the grey value profiles (Fig. 3.5). A fixed profile is not necessarily characteristic for one region/patch, but a region has certain features for the grey values, because of its position relative to other brain structures. For example there is no neighbouring structure near the lip region, such that it shows high bright-dark contrast. In this region the boundary of the calyx is easily detectable by a minimum in the derivative. (Fig. 3.5, profile 1).

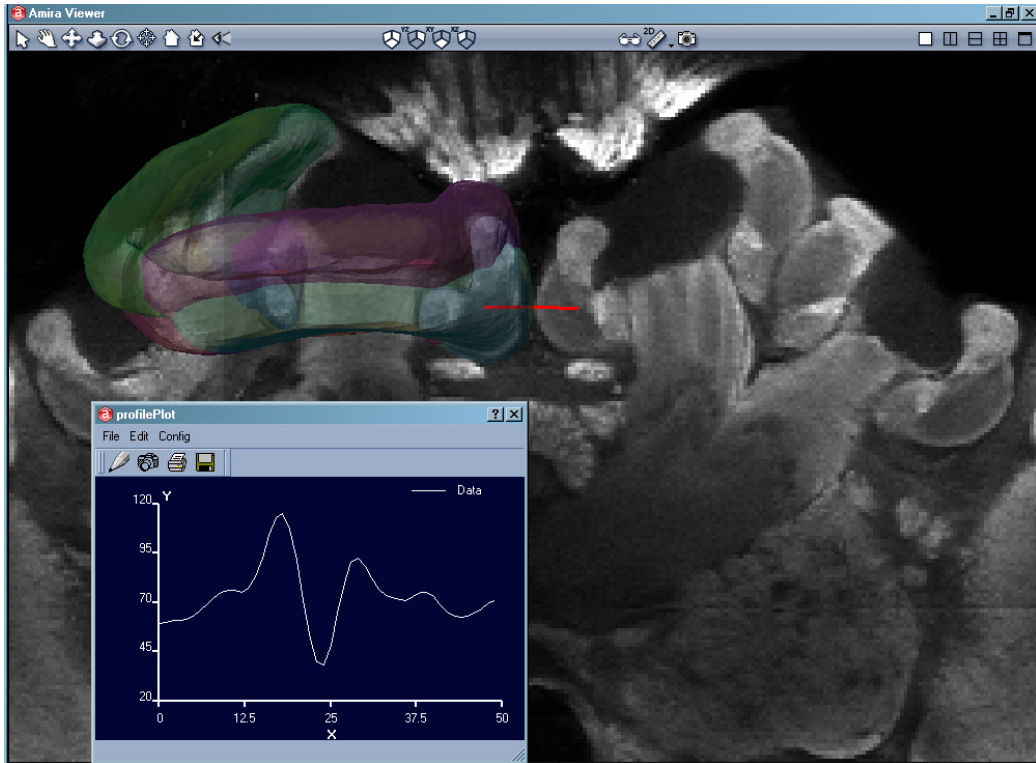


Figure 3.4: Analysis of grey value profiles with Amiras ExamineProfileEditor

3.4 Displacement algorithm

Since the confocal images of the bee brains show uneven staining, it is not possible to find a constant threshold value for a thresholding displacement algorithm. For example mostly the lip is very bright and the collar is relatively dark. I tried to define region specific intensities for the inside of the calyx for each defined patch. But this is difficult because of an intensity gradient in depth of the confocal image stack. It worked better when the threshold value is approximated from the actual profile. If there is a large contrast between inside and outside grey values, the threshold value lies approximate in the middle of the maximum and minimum grey value. Therefore in this case the algorithm is independent of any gradient in depth. An additional feature of the images from synapsin stained bee brains are intense edges (see collar in Fig.3.4). However, an algorithm, which uses only edge information all the

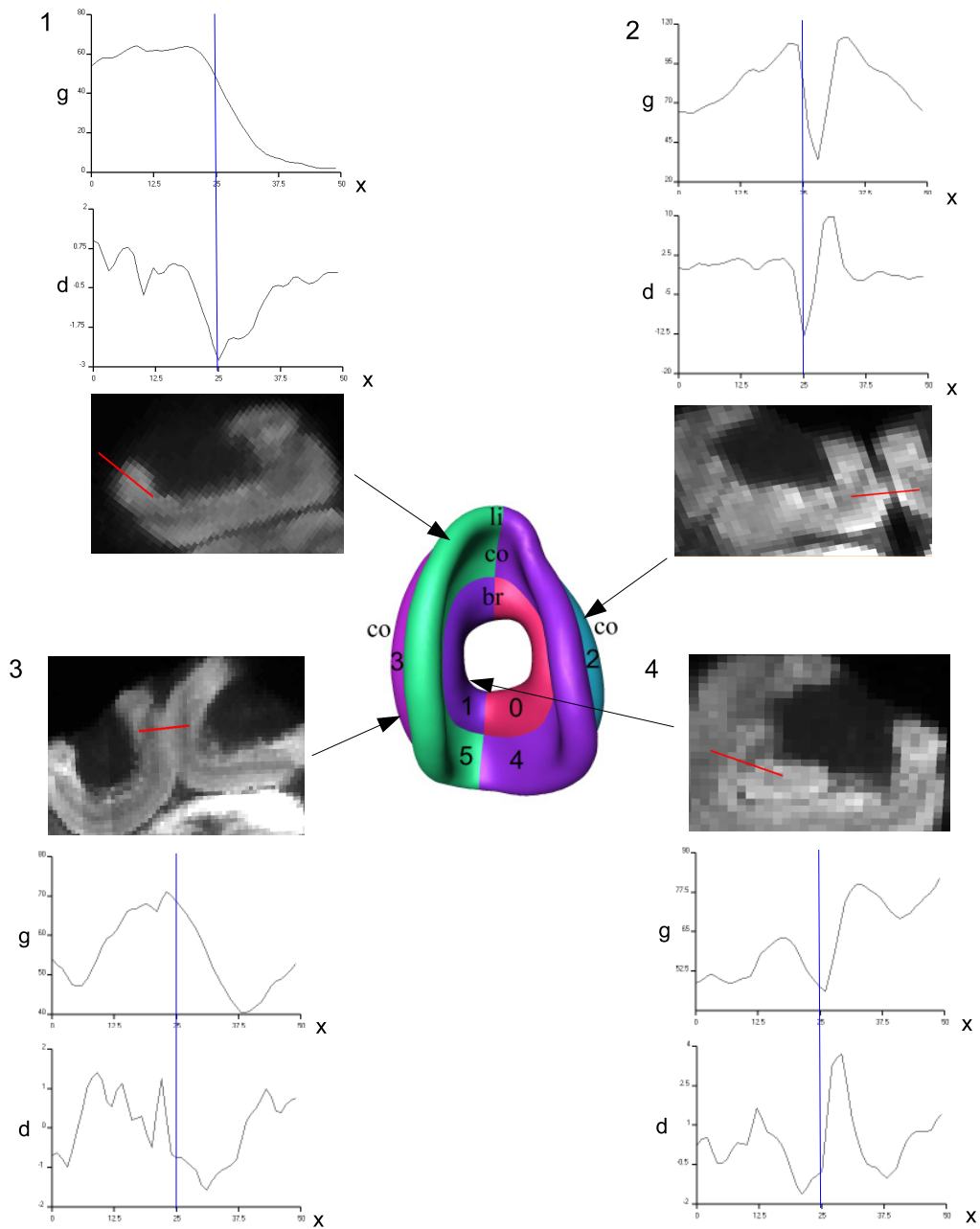


Figure 3.5: Grey value profiles (g) and their derivatives (d) with a length of $100 \mu\text{m}$ along vertex normals and corresponding oblique slices with 1D profile in red (x is the position in the profile). In 1-4 profiles of the same dataset are shown, the blue line marks the boundary of the calyx surface: 1: in lip region (li) strong bright-dark contrast and edges (minimum in derivative). 2: in collar region (co), neighbouring to left median calyx, boundary at a bright-dark transition of grey values, where the derivative reaches its minimum. 3: in collar region, neighbouring to the right lateral calyx, the boundaries of the structures are fused with bright grey values in the middle (maximum of profile). 4: basal ring (br), nearby peduncle, inside darker than outside, between the maxima a narrow minimum in the profile.

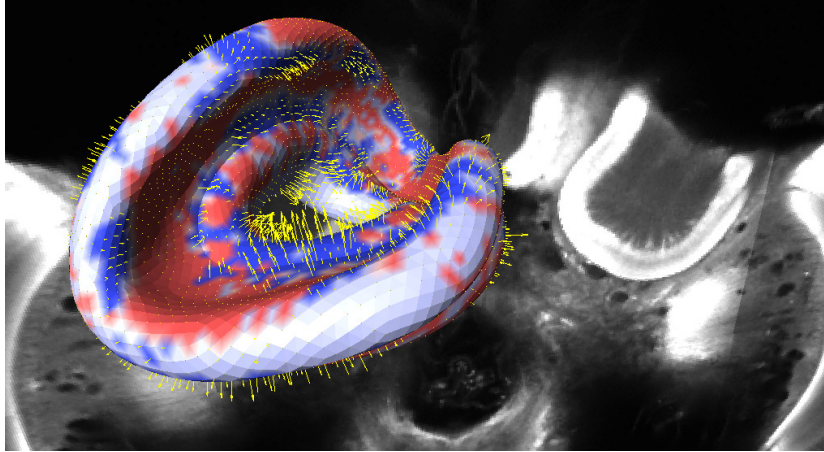


Figure 3.6: Displacement of the calyx model in the image data, blue color means the displacement vectors point outwards, red means they point inwards, displacement vectors shown as yellow arrows.

time, does not work reliable, because closely neighbouring structures have also strong edges and sometimes there are no edges at all. Further problem is the low contrast and weak edges within the mushroom body and at the boundary towards basal ring, peduncle and the boundary towards the neighbouring lateral calyx. The model-based method could compensate for the lack of utilizable information in these profiles. A combination of a thresholding with the edge detection improved the segmentation result, but the boundary between calyx and peduncle remains difficult to detect, because peduncle and basal ring are both bright and between them there is a faint dark edge (see Fig. 3.5, profile 4). There are also difficulties if the proto-cerebral lobe is positioned nearby the collar, which is much more brighter and has stronger edges than the collar boundary or if the boundary of the lateral calyx is too close. The algorithm should treat these cases separately, such that the model will not be guided into neighbouring structures or adjusted to wrong edges in the image. These problems lead to the following algorithm, which should detect the described cases and choose between the fitting displacement strategy. It needs information about the intensity of the grey values of the actual picture, because they are varying between different confocal scans.

Therefore after the Initialization and a rigid adjustment of the model the parameters for the displacement algorithm (except the absolute gradient value) are computed through a histogram analysis of the gray values inside the calyx. The histogram analysis, which is implemented in Amira, computes the frequency of grey values. It can also compute a reverse thresholding, which I expect to result in an approximation of the minimal grey value outside the calyx and the maximal grey value outside the calyx.

In the segmentations performed below, I estimated the minimal grey value outside the calyx as the grey value, which at least 90% of the voxels reach. The maximal grey value outside the calyx represents the grey value of more brighter neighbouring structures (protocerebral lobe and neighbouring calyces). I used the grey value, which 5% of the grey values reached. The mean grey value was the computed mean grey value of all voxels.

Parameter

- mean grey value of calyx (\bar{g})
- minimal grey value outside of calyx (outMin)
- maximal grey value outside of calyx (outMax)
- absolute gradient (absDiff)

Let $g(i)$ be the grey value at position i in the profile, and px the position in the middle of the profile. At first the maximal grey value (g_{max}), the minimal grey value (g_{min}), the maximal value (d_{max}) and the minimal value of the derivative (d_{min}) and their indices are computed from the profile. In the following section I describe each step of the algorithm.

displacement algorithm

The calyx is brighter than the outside, if no neighbouring structure is close.

1a) if $g(px) > \bar{g}$:

It is likely, that px lies inside the calyx, it should search outwards until it finds a local minimum in the profile with a grey value less than the average grey value of the structure, i.e. find the index $i_{locMin}, (i_{locMin} > px)$ with $g(i_{locMin}) < \bar{g}$ and $g(i_{locMin} + 1) > \bar{g}$,

1b) if $g(px) < \bar{g}$:

It is likely, that px lies outside the calyx, search inwards until a grey value larger than the mean calyx grey value is found, i.e. find $i_{locMin}, (i_{locMin} < px)$ with $g(i_{locMin}) < \bar{g}$ and $g(i_{locMin} - 1) > \bar{g}$, if there is a $j > px$ with $g(j) > \bar{g}$.

2.a) if i_{locMin} was found in 1. assume that a local maximum further inside lies within the calyx, find the local maximum i_{locMax} with $i_{locMax} < i_{locMin}$.

2.b) if $g_{max} > outMax$ and $(i_{min} < i_{max})$:

If the absolute maximum of the profile is bigger than a threshold and the absolute minimum lies further inside than the maximum, there might be a brighter adjacent structure e.g. neighbouring calyx or somata. Between the structures there should be a local minimum. The boundary of the calyx lies then further inside of the minimum, between the local minimum and a local maximum.

It searches for a local minimum i_{locMin} with $i_{locMin} < i_{max}$ and the next local maximum i_{locMax} further inside with $i_{locMax} < i_{locMin}$.

3.) The boundary of the calyx lies approximately in the middle of the found local minimum and maximum, i.e. go to $px = \frac{1}{2}(i_{locMin} + i_{locMax})$.

4.) To find the edge of the calyx, the local minimum of the derivative is searched with $locMinD > absDiff$.

5.) If case 2a or 2b are not right, and the gradient in the profile is very

low, try a thresholding adjustment with $threshold = \frac{1}{2}(g_{min} + g_{max})$. Then go to local minimum of the profile.

6.) If the gradient is very strong:

6a) If $g_{max} > outMin$ und $i_{max} < i_{min}$ and the absolute value of the maximum of the derivative is larger than the one of the minimum ($|d_{max}| > |d_{min}|$): go directly to the absolute maximum of the derivative.

6b) if the condition under 6a) is not fulfilled, go directly to the absolute minimum of the derivative.

Chapter 4

Results

The outcome of the described automatic segmentation process of confocal image data depends on three components:

1. The affine registration of the particular grey value dataset to the Standard grey value dataset, which initializes the position of the model in the grey value dataset.
2. The ability of the gray value profile model to suit for synapsin stained confocal test datasets.
3. The ability of the model to adjust to arbitrary shapes, i.e. the completeness of the model

The affine registration to the Standard grey value dataset was performed for 45 confocal 3D image stacks from synapsin stained bee brains. 18 of the tested datasets are the basis of the honey bee Standard brain atlas. For all datasets the affine registration worked, such that the transformation parameters could be used for an approximate positioning of the model in the region of the right median calyx in the confocal dataset.

The ability of the developed profile model to adapt to profiles of arbitrary grey value datasets is tested by the segmentation of the mentioned confocal

datasets from which the model was made (Leave-all-in segmentation test). The segmentation process is therefore independent of the model. It depends only on the profile model and the segmentation strategy.

The compactness of a statistical shape model is defined as the number of shape modes, which it needs at least to describe the variability of a shape. The completeness of a statistical shape model is its ability to adjust to arbitrary shapes (generalization ability).

To improve the completeness of the calyx model, I extended it with 27 shapes. Then I performed the automatic segmentation of the 45 confocal datasets with different sized models including 18, 34 and 45 training shapes. The grey value datasets were the same used for the modeling process, but for the performed segmentation test the respective shape was removed from the model (Leave-one-out segmentation Test).

To evaluate the results of the automatic segmentations (Leave-all-in and Leave-one-out segmentation tests), the manual segmentation is used as a gold-standard. The following distance measures are used to compare the automatic and manual segmentation result. They are either based on 2-sided distances of surfaces or Volume overlaps of label fields.

4.1 Evaluation

The following surface distance measures are two-sided distance measures. The distance $d(x, S')$ between a point x on a surface S and the surface S' is the minimum over the normed distances of the point x of S and all points x' in S' , where $\|\cdot\|_2$ is the euclidean norm:

$$d(x, S') = \underbrace{\min}_{x' \in S'} \|x - x'\|_2$$

$|S|$ is the area of the surface S .

4.1.1 Symmetric surface distance

Mean Distance

The mean distance of two surfaces is defined as the sum over the distances of all points of the surface S to the surface S' plus the sum over the distances of all points of S' to S , divided by the sum of the areas of the surfaces:

$$d_{mean}(S, S') = \frac{1}{|S| + |S'|} \left(\int_{x \in S} d(x, S') dS + \int_{x' \in S'} d(x, S) dS \right)$$

Root Mean Square Distance

The root mean square distance of two surfaces is the root of the normed sum of the squared distances of all points of the surface S to the surface S' and all points of the surface S' to S .

$$d_{RMS}(S, S') = \sqrt{\frac{1}{|S| + |S'|} \left(\int_{x \in S} d(x, S')^2 dS + \int_{x \in S'} d(x, S)^2 dS \right)}$$

Maximum Distance

The maximum distance of two surfaces is defined as the maximum of the maximal distance of the surface S' to the points of the surface S and the maximal distance of the surface S to the points of the surface S' .

$$d_{max}(S, S') = \max \left(\underbrace{\max}_{x \in S} d(x, S'), \underbrace{\max}_{x \in S'} d(x, S) \right)$$

4.1.2 Volume overlap

To compare the overlap of the label fields of the automatic and manual segmentation, the symmetric volume difference of the label fields is measured.

The labelfield of the automatic segmentation is computed by sampling the interior of the surface on a regular grid using scan conversion with the original confocal dataset as grid.

$$v_{overlap}(S, S') = \frac{2|V_S \cap V_{S'}|}{|V_S| + |V_{S'}|}$$

4.2 Segmentation of training data

To evaluate the profile model I performed an automatic segmentation of 45 confocal datasets, which are included in the model (Leave-all-in segmentation). In Fig. 4.1 the four steps of the segmentation process is shown. The outcome of the segmentations is very different for single datasets (fig.4.3). For 28 out of 45 (62%) the result is very good with respect to the mean surface distance, which is $\leq 3.5\mu m$ and the volume overlap $\geq 92\%$. For another 10 datasets (20%) the result is good: surface distances $< 4.4\mu m$ and volume overlaps $\geq 90\%$. For the remaining datasets the result is worse, for 5 of them the mean surface distance is bigger than $5\mu m$ and the volume overlap ranges between 83% and 89%. For 2 datasets the profile model fails, for the other ones the mean distances of the surfaces and label fields of the automatic and manual segmentations are evaluated with the distance measures in section 1. Often the maximal surface distances are very large ($26.7 \pm 11.8\mu m$). The mean surface distance of the result and the gold standard is $3.5 \pm 1.1\mu m$. The mean Volume overlap of the label fields of the manual and automatic segmentation is 92%. The datasets, for which the profile model failed, do not belong to the Standard data. However, excluding these outsiders, the segmentation did not work better for the Standard data (mean surface distance $3.7\mu m$ compared to $3.4\mu m$ for the other datasets).

Segmentation Tests				
	$d_{mean} [\mu m]$	$d_{RMS} [\mu m]$	$d_{max} [\mu m]$	$v_{overlap} [\%]$
Leave-all-in (45)	3.5 ± 1.1	4.8 ± 1.7	26.7 ± 11.8	92.0 ± 2.4
Leave-one-out (17)	5.3 ± 1.5	6.9 ± 2.2	31.8 ± 13.3	87.8 ± 4.0
Leave-one-out (33)	4.4 ± 0.9	5.8 ± 1.3	29.4 ± 10.7	89.9 ± 2.3
Leave-one-out (44)	4.5 ± 1.0	6.1 ± 1.6	33.0 ± 12.0	89.7 ± 2.4
Leave-one-out (44) F	4.0 ± 1.0	5.9 ± 1.6	34.4 ± 12.3	90.9 ± 2.2
Shape model optimization Test				
Leave-one-out (44)	3.0 ± 0.6	3.8 ± 0.8	17.7 ± 4.5	93.2 ± 0.02

Table 4.1: Average two-sided surface distances and volume overlaps of label fields between manual and automatic segmentation of the Leave-all-in and Leave-one-out segmentations with different sized models (number of training shapes of the used model in brackets), in the last row of the segmentation tests a free form deformation step allows the model to deform beyond its shape captured by the training data. Below the result of the shape model optimization test with a model containing 44 training shapes is displayed.

4.3 Extension of the calyx model

4.3.1 Compactness of the calyx model

Increasing the number of training shapes contained in the model enlarges the number of shape modes, i.e. a larger model has more degrees of freedom. The original statistical shape model of the calyx was made of 18 training shapes, resulting in 17 shape modes. The enlarged model consists of 45 training shapes, i.e. 44 shape modes. I want to figure out how many of the shape modes are at least needed to describe the shape of the training data (compactness of the model). The smaller model needs 12 out of 17 modes to cover 95% of its total variance, i.e. 70% of the shape modes are sufficient to describe the shape of the training data (Fig. 4.2). The extended model needs 23 shapes out of 44 shape modes to describe the variance of the training data, i.e. 52% of the total number of shape modes (Fig. 4.2). Thus the model made of 45 training shapes has increased compactness compared to the smaller model made of 18 shapes. This result means, that theoretical not all 44 have to be included in the segmentation process, 23 shape modes

should be sufficient.

4.3.2 Completeness of the calyx model

The ability of the model to describe arbitrary shapes (completeness) can be tested by a shape optimization to its training shapes. Therefore each of the 45 training shapes is removed separately from the model and then the model consisting of the remaining 44 shapes is matched to the removed shape by the computation of a rigid transformation and shape parameters which minimize the symmetric root mean square distance between the model and the particular surface. An arbitrary shape can be described by the model with a mean surface distance of $3.0 \pm 0.6\mu m$ and maximal surface distance of $17.7 \pm 4.5\mu m$ (see Tab. 4.1). This number is a lower bound for the segmentation result using the model with 45 training shapes. Even with the best suited profile model and displacement algorithm, this boundary would not be exceeded.

4.4 Segmentation of arbitrary test data

In order to automatically segment arbitrary datasets, the model should be able to adjust to arbitrary shapes and the profile model should be suitable for profiles of the particular dataset. To test this generalization ability of the model made of 45 training shapes and the profile model one shape of the training shapes is removed and then the segmentation is performed with the reduced model. The performed test is called Leave-one-out segmentation, because the tested dataset is not contained in the model. The result depends on both the profile model and the variability of the model. The profile model fails in two datasets. They were excluded from the computation of the mean surface distances in Tab. 4.1. Fig. 4.3 shows the surface distances of the Leave-all-in and Leave-one-out segmentation for the remaining 43 datasets. The mean surface distance of the Leave-one-out segmentation is $4.5 \pm 1.0\mu m$

compared to $3.5 \pm 1.1 \mu m$ in the Leave-all-in segmentation. The mean volume overlap of the Leave-one-out segmentation is about 90% and for the Leave-all-in segmentation 92%, see Tab. 4.1. In the Leave-one-out segmentation test incorrect segmentations occurred at the boundary of the calyx to the peduncle and the lip boundary. The segmentation of the boundary to the peduncle was even incorrect in the Leave-all-in segmentations, where the lip-boundary was correct (see example in Fig. 4.4). To improve the adjustment of the model in the lip-regions I tested a free form deformation step at the end of the described segmentation procedure. It turned out to improve the overall segmentation result, with a mean surface distance to the manual segmentation of $4.0 \pm 1.0 \mu m$ compared to $4.5 \pm 1.0 \mu m$ without the free form deformation step. However, the maximum surface distance is larger: $34.4 \pm 12.3 \mu m$ compared to $33.0 \pm 12.0 \mu m$. The volume overlap of the label fields improved to 90.9 ± 2.2 compared to $89.7 \pm 2.4\%$. I compared the segmentation results obtained with and without the free form deformation step. In regions, where the profile model fits, e.g. the lip boundary and parts of the collar region, the free form deformation improves the segmentation result. But in parts of the calyx, e.g. near the peduncle or the neighbouring left calyx the result gets worse (see example in Fig. 4.5).

I asked whether the segmentation result becomes better with a larger model. Therefore I performed the Leave-one-out Test with 45 training data and models with 17, 33 and 44 training shapes. The result is displayed in Tab. 4.1. The original model made of 18 training shapes reached a mean surface distance of manual and automatic segmentation of $5.2 \pm 1.4 \mu m$. The extended model with 34 shapes performs better ($4.4 \pm 0.9 \mu m$). The largest model with 45 shapes can not perform better than the model with 34 shapes. Fig.4.6 shows the volume overlap between manual and automatic segmentations for the segmentations with the smaller model (17 training shapes) and the enlarged model (44 training shapes) of 45 confocal datasets. In most cases the larger model performs better. For the Standard data the segmentations obtained with the different models is very similar. It seems, that the segmentation result for the Standard data is better than for the other datasets.

The average surface distance of the Standard data compared with the average surface distance of the other datasets is similar, but the non Standard data show higher variability in their segmentation results.

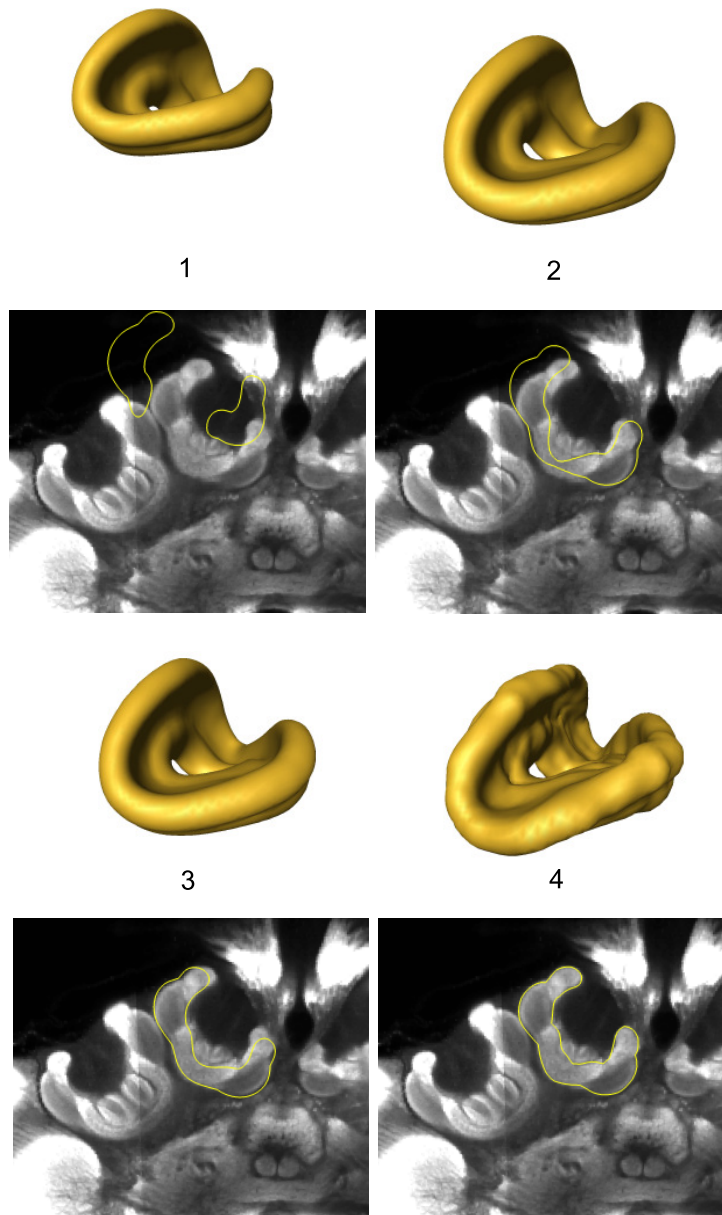


Figure 4.1: The four steps of the segmentation process for a dataset contained in the model is shown. 1: initial positioning of the mean model in the confocal dataset. 2: result of the affine registration of the confocal dataset to the Standard reference dataset. 3: result of the rigid transformation of the model. 4: result of the optimization of position and shape parameters of the model.

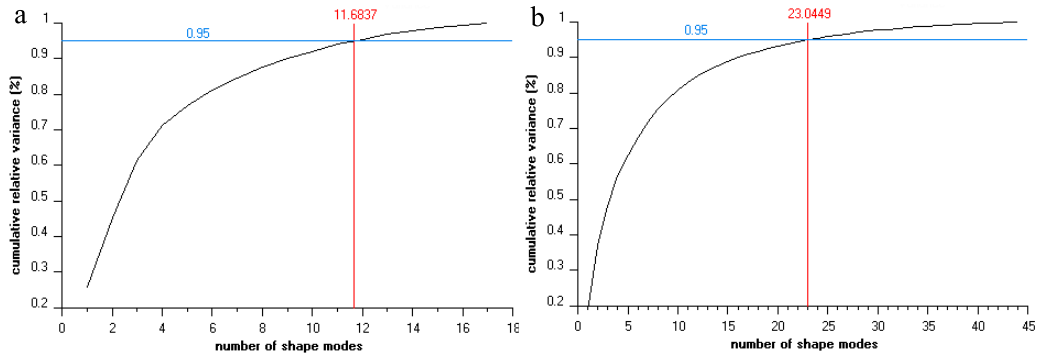


Figure 4.2: Cumulative relative variance of the model containing 18 (a) and 45 (b) training shapes.

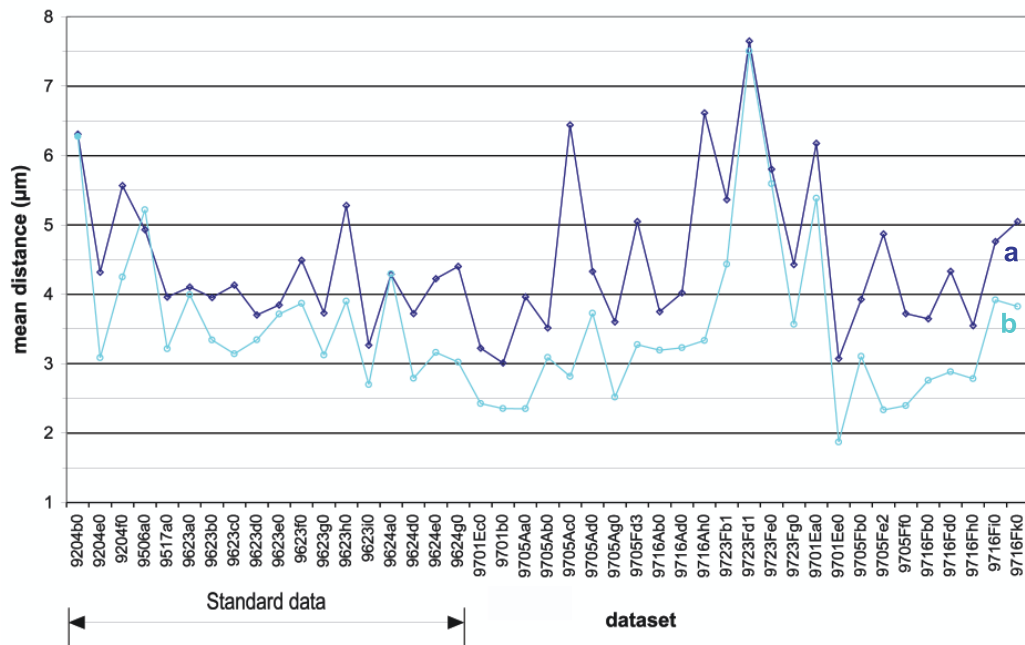


Figure 4.3: Comparison between surface distances from manual and automatic segmentation for a segmentation with the model containing the segmented dataset (Leave-all-in Test: b) and not containing it (Leave-one-out Test: a). The results for the segmentation of 43 confocal datasets with a shape model with 45 (a) and 44 (b) training shapes are displayed.

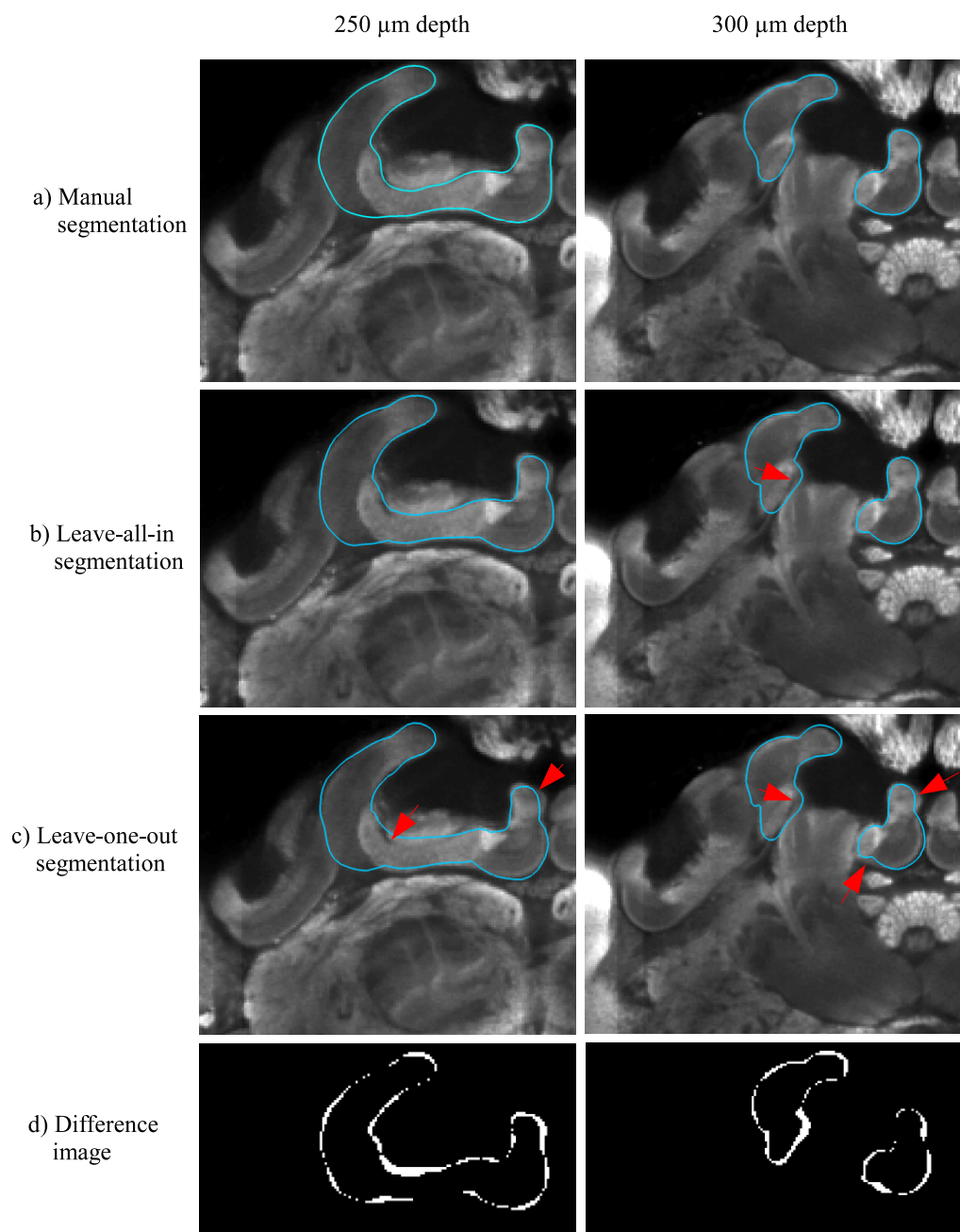


Figure 4.4: In two depths of the image stack the manual (a) and the automatic segmentations (b,c) and the difference image of (a) and (c) are shown. Incorrect autosegmented regions are marked with a red arrow. The mean surface distance between manual and Leave-one-out segmentation is $4.13\mu\text{m}$ and the volume overlap of the corresponding label fields is 91.1%.

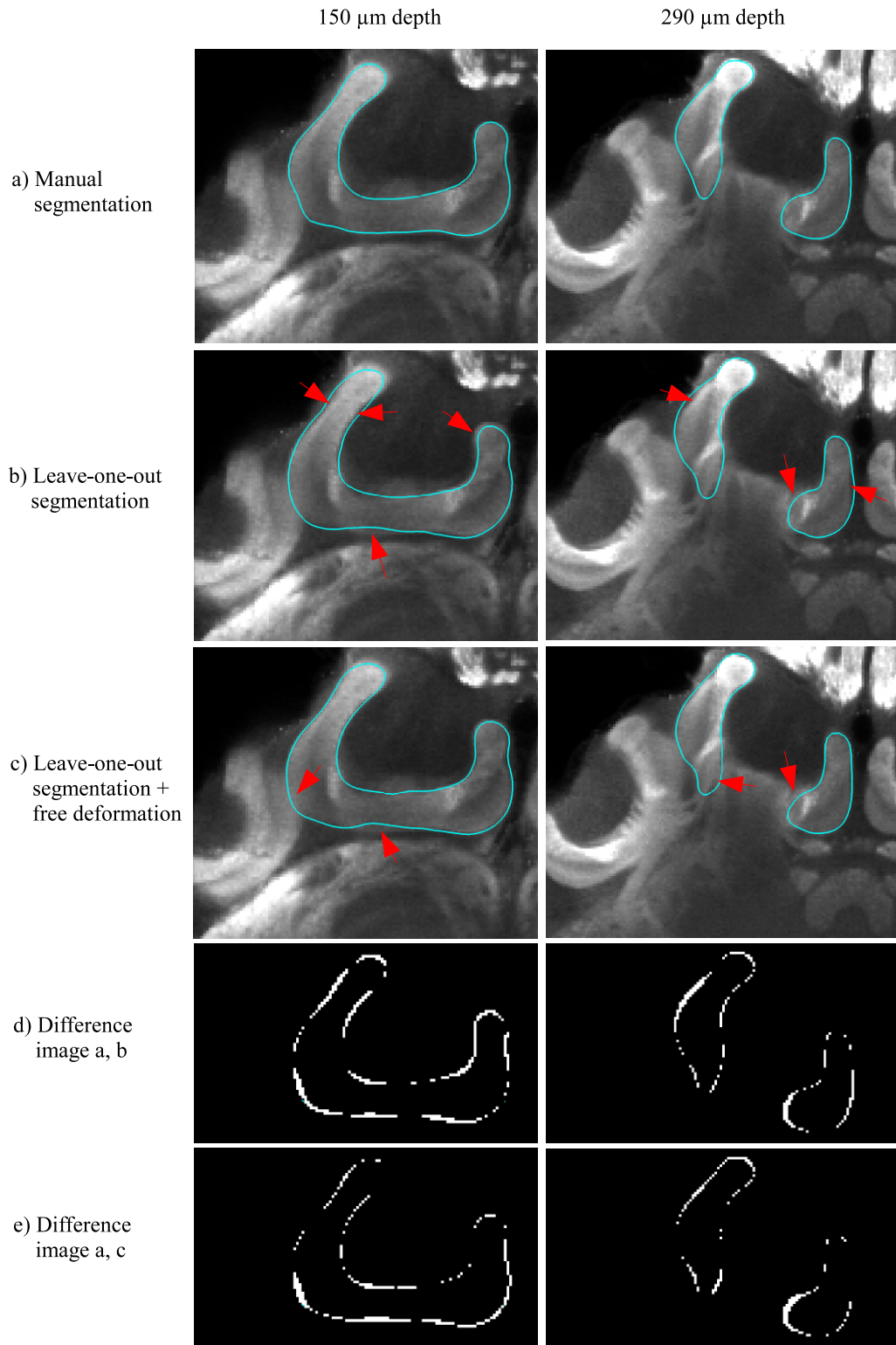


Figure 4.5: In two depths of the image stack the manual (a) and automatic segmentations (b,c) and the difference image of a,b and a,c are shown. Incorrect autosegmented regions are marked with a red arrow.

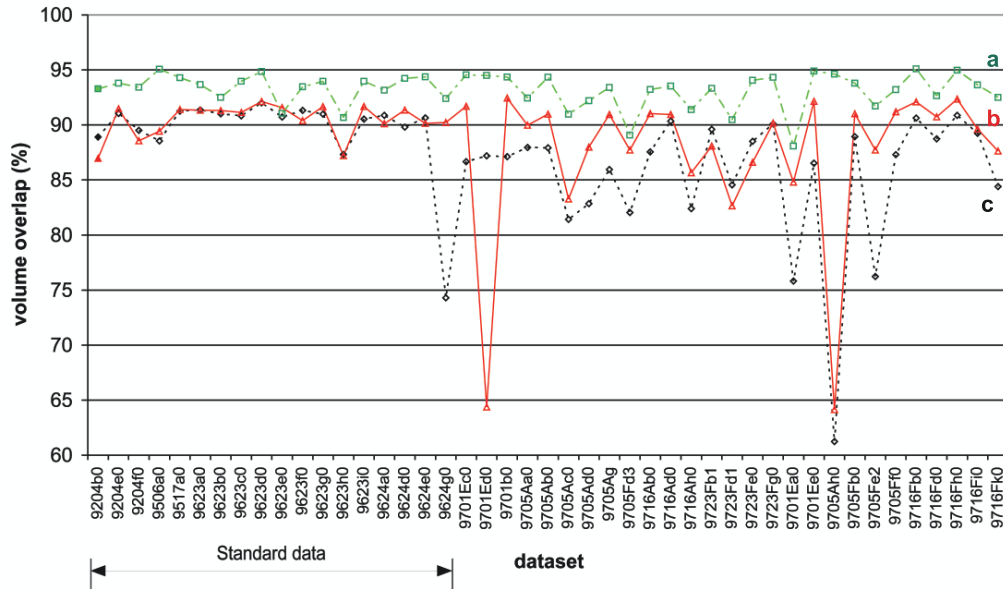


Figure 4.6: Comparison between the volume overlap of manual and automatic segmentation for the Leave-one-out segmentation using different sized models containing 44 (b) and 17 (c) training shapes. The results for the segmentation of all tested 45 confocal datasets are displayed, the first 18 datasets belong to the Standard data. The upper bound for the volume overlap which can be achieved with the model containing 44 shapes is the result of the shape model optimization to the datasets (a).

Chapter 5

Discussion

In principle the profile model fits for the tested confocal datasets: 80% of the datasets have surface distances $\leq 4.4\mu m$ and volume overlaps $\geq 90\%$ in the Leave-all-in segmentation test (Tab.4.1, Fig. 4.3). The large maximal surface distances indicate, that in some regions of the calyx, the profile model makes mistakes.

The completeness of the extended model with 45 training shapes was tested in a shape model optimization test (Leave-one-out test). With a perfect fitting profile model this statistical shape model would be able to adjust to arbitrary shapes with a mean surface distance of $3.0 \pm 0.6\mu m$ and a root mean square distance of $3.8 \pm 0.8\mu m$, which would result in a volume overlap of 93%. The root mean square distance in the Leave-all-in segmentation is larger than the root mean square distance of the Leave-one-out test of the computed shape model optimization ($4.8\mu m$ versus $3.8\mu m$). I expected it to be smaller, because in the Leave-all-in segmentation test the segmented shape is contained in the model. This fact demonstrates, that the profile model should be improved.

The result of the Leave-one-out segmentations could be improved with a larger model containing 33 training shapes compared to 17 training shapes. A further extension could not produce better results. In some cases the

result becomes even worse with the model containing 44 shapes compared to the ones with a model containing 33 shapes, such that the mean maximal surface distance and the RMS distance is bigger (see tab.4.1). The fact that the results can get worse with more degrees of freedom of the model reveals some weakness of the profile model.

It is very difficult to find a profile model, which suits the segmented confocal datasets in different preparations. The staining of the confocal images is varying, such that the intensity and contrast can be different. The segmentation result for the Standard data was less variable than for the other data. It was similar using the model with 17 shapes and the one with 44 shapes (Fig. 4.6). There are different possible reasons for that effect. The first is the fact, that these Standard data sets were included in the computation of the average Standard grey value dataset, which I used as the reference dataset for the affine registration of the individual grey value datasets for the initialization of the model. I have not measured, if the outcome of the affine registration was significantly better than for the other datasets. But since in the performed segmentations the model boundary did not move far away from the calyx boundary, I suppose that the effect of different initialization results would be small. The second reason could be, that the staining of the different preparations of the bee Standard dataset is more reliable than for the remaining datasets. The third possible reason could be, that the shape of the calyces of the original model with 18 training shapes are very similar to each other and differ very much from the shape of the calyces which I added to the model.

In some segmentations, the statistical shape model was not able to adjust to the individual shape, especially at the borders of parts of the lip and the collar. Except for some regions e.g. near the peduncle, where it is difficult to detect the boundary of the calyx during profile analysis, a free form deformation step at the end of the segmentation process could improve the result (Fig. 4.5). The mean surface distance were $4.0\mu\text{m}$ compared to $4.5\mu\text{m}$ without the free form deformation step (volume overlap 91% and 90%). The result might be even better, if it could be avoided that a deformation

occurs in regions where the profile does not contain enough information. That could be done by a region-specific free form deformation approach.

Chapter 6

Conclusions and Outlook

In this work I used a heuristic approach to model grey value profiles of very divergent datasets. I tried to model varying profiles in the analysed grey value datasets. It turned out to be difficult to consider all found profiles in a displacement algorithm. Therefore I would suggest to model the features of the grey value profiles via a statistical analysis e.g. clustering method. The displacement algorithm could then choose the suitable displacement by a kind of comparison of the features of the actual profile and the modeled profiles. I think the variability of the extended statistical shape model of the calyx would be sufficient to use it for the automatic segmentation of confocal image data. A free form deformation step can be used to improve its adaptation to individual calyx shapes in highly variable regions e.g. the lip.

The model-based segmentation depends on the chosen staining technique. Even with a given staining method, here immuno-stained, the segmented confocal image datasets vary in their grey values. This results in variable outcome of the automatic segmentation (Fig. 4.6).

Despite of the described difficulties arising with confocal image data, the described model-based segmentation approach has some advantages. It uses a-priori information about the segmented shape and can therefore compensate for the different background knowledge of a particular brain structure

of the human segmenters. Even with a slightly incomplete segmentation result less time would be needed for the correction than with semi-automatic segmentation.

Bibliography

- [1] Robert Brandt, Torsten Rohlfing, Juergen Rybak, Sabine Kroficzik, Alexander Maye, Malte Westerhoff, Hans-Christian Hege, and Randolph Menzel. Three-dimensional average-shape atlas of the honeybee brain and its applications. *The Journal of Comparative Neurobiology*, 492:1–19, April 2005.
- [2] Hans Lamecker, Thomas Lange, and Martin Seebass. Segmentation of the liver using a 3d statistical shape model. *ZIB-Report*, 04-09, April 2004.
- [3] Hans Lamecker, Martin Seebass, Hans-Christian Hege, and Peter Deuffhard. A 3d statistical shape model of the pelvic bone for segmentation. *Proc. of SPIE-Medical Imaging*, 5370, 2004.
- [4] A. Maye, T.H. Wenckebach, and H.-C. Hege. Visualization, reconstruction, and integration of neuronal structures in digital brain atlases. *International Journal of Neuroscience*, 116:431–451, 2006.